© 2018. Published by The Company of Biologists Ltd | Development (2018) 145, dev160739. doi:10.1242/dev.160739

RESEARCH REPORT

Nppa and Nppb act redundantly during zebrafish cardiac development to confine AVC marker expression and reduce cardiac jelly volume

Daniela R. Grassini, Anne K. Lagendijk, Jessica E. De Angelis, Jason Da Silva, Angela Jeanes, Nicole Zettler, Neil I. Bower, Benjamin M. Hogan and Kelly A. Smith*

ABSTRACT

Atrial natriuretic peptide (*nppa*/*anf*) and brain natriuretic peptide (*nppb*/*bnp*) form a gene cluster with expression in the chambers of the developing heart. Despite restricted expression, a function in cardiac development has not been demonstrated by mutant analysis. This is attributed to functional redundancy; however, their genomic location *in cis* has impeded formal analysis. Using genome editing, we have generated mutants for *nppa* and *nppb*, and found that single mutants were indistinguishable from wild type, whereas *nppa*/*nppb* double mutants displayed heart morphogenesis defects and pericardial oedema. Analysis of atrioventricular canal (AVC) markers show expansion of *bmp4*, *tbx2b*, *has2* and *versican* expression into the atrium of double mutants. This expanded expression correlates with increased extracellular matrix in the atrium. Using a biosensor for hyaluronic acid to measure the cardiac jelly (cardiac extracellular matrix), we confirmed cardiac jelly expansion in *nppa*/*nppb* double mutants. Finally, *bmp4* knockdown rescued the expansion of *has2* expression and cardiac jelly in double mutants. This definitively shows that *nppa* and *nppb* function redundantly during cardiac development to restrict gene expression to the AVC, preventing excessive cardiac jelly synthesis in the atrial chamber.

KEY WORDS: ANF, Cardiac development, Nppa, Cardiac jelly, Zebrafish

INTRODUCTION

At early stages of development [24-30 h post fertilisation (hpf) in the zebrafish], the heart is a double-layered linear tube, with an inner layer of endothelium (called the endocardium) and an outer muscular layer called the myocardium. During cardiac morphogenesis in both zebrafish and mice, the prospective atrial and ventricular chambers of the heart 'balloon' out of the heart tube, becoming morphologically and genetically distinct from the atrioventricular canal (AVC). The AVC is a specialised region of the developing heart that partitions the two chambers. It is characterised by *Bmp2/4* (Keyes et al., 2003; Ma et al., 2005; Walsh and Stainier, 2001) and *Tbx2* (Chi et al., 2008; Christoffels et al., 2004; Harrelson et al., 2004) gene expression in the myocardium and *Has2* gene expression in the endocardium (Tien and Spicer, 2005). *Has2* encodes a synthetic enzyme of the extracellular matrix component, hyaluronic acid (HA), and, congruent with its expression, localised swellings of extracellular matrix (ECM; known as 'cardiac jelly') are observed at the AVC. These swellings are the endocardial cushions: primitive structures that will later remodel to form cardiac valve leaflets.

The hierarchical relation between *Bmp2/4* and *Tbx2* has been extensively described, both in fish and mammals. *Bmp2/4* and *Tbx2* depletion share the phenotype of impaired AV boundary establishment (Chi et al., 2008; Harrelson et al., 2004; Ma et al., 2005) and reduced Bmp signalling results in undetectable expression of *Tbx2* in the AVC myocardium, placing Bmp signalling upstream of *Tbx2* (Ma et al., 2005; Shirai et al., 2009; Verhoeven et al., 2011). The zebrafish *jekyll* mutant, which harbours a mutation in the UDP-glucose 6-dehydrogenase gene (another enzyme of the HA biosynthetic pathway), and *Has2*-null mice show a key function for the cardiac jelly in determining both correct patterning and early localised growth of the endocardial cushions (Camenisch et al., 2000; Walsh and Stainier, 2001).

Although *Bmp2/4* and *Tbx2* are restricted to the AVC, *Nppa* (also known as ANF, atrial natriuretic factor) and *Nppb* (also known as BNP, brain natriuretic peptide) represent their chamber myocardium counterpart: *Nppa* and *Nppb* expression are enriched in the ballooning surfaces of the cardiac tube, and *Nppa* is actively excluded from the AVC by the repressive function of *Tbx2* (Becker et al., 2014; Christoffels et al., 2004; Habets et al., 2002). Despite their compelling expression patterns, little has been reported about the function of *Nppa* and *Nppb* during heart development. *Nppa*- or *Nppb*-null mice lack any obvious developmental phenotype (John et al., 1995; Tamura et al., 2000). *Nppa* and *Nppb* lie in a conserved gene cluster (Inoue et al., 2003; Tamura et al., 1996) with common regulatory regions that become activated during development (Sergeeva et al., 2016). This co-regulation, their homology and the absence of developmental phenotypes observed in response to single gene loss of function has led to the hypothesis that these two genes are functionally redundant.

Here, we describe the generation of single and double *nppa* and *nppb* zebrafish mutants, which is now possible with genome-editing methods. Consistent with previous reports, single mutants exhibit no overt developmental phenotype. In contrast, double mutants exhibit pericardial oedema, expanded AVC markers and thickening of the cardiac jelly in the atrium of the early embryonic heart. These data support the notion that *nppa* and *nppb* function redundantly, and demonstrate that *nppa/nppb* double mutants play a previously unappreciated role in cardiac development by restricting AVC gene expression and repressing ECM accumulation in the atrial chamber.

Institute for Molecular Bioscience, The University of Queensland, Brisbane, Queensland 4072, Australia.

*Author for correspondence (k.smith@imb.uq.edu.au)

D.R.G., 0000-0003-4744-8278; A.K.L., 0000-0003-1246-1608; J.E.D., 0000-0003-3326-6975; B.M.H., 0000-0002-0651-7065; K.A.S., 0000-0002-8283-9760

Received 19 October 2017; Accepted 2 May 2018

Development (2018) 145, dev160739. doi:10.1242/dev.160739

RESULTS AND DISCUSSION

nppa and *nppb* act redundantly during early cardiac morphogenesis

In zebrafish, the *nppa* and *nppb* loci reside in a gene cluster on chromosome 8, separated by approximately 2.5 kb (Fig. 1A). This proximity precludes a classical strategy of generating double homozygous mutants by homologous recombination. To overcome this, we undertook sequential mutagenesis of the two loci, first generating an *nppa* mutant line using TALEN technology, and then targeting the *nppb* locus in the *nppa* mutant background using the CRISPR/Cas9 system. Simultaneously, *nppb* single mutants were created. For *nppa*, exon 1 was targeted, producing a 4 bp deletion at 55 bp of the coding region (*nppa*^{uq19ks}). This results in normal protein sequence until amino acid 18, followed by frameshifted sequence to amino acid 23 and then translational termination (Fig. 1A,B), preventing generation of the 139 amino acid wild-type protein. For *nppb*, exon 2 was targeted and two alleles were generated. The mutant locus *nppb*^{uq20ks}, which is linked *in cis* to the *nppa*^{uq19ks} allele, carries a 39 bp insertion containing a stop codon, resulting in a shorter protein of 80 amino acids (Fig. 1A,B; full-length wild-type protein contains 129 amino acids). The single *nppb*^{uq21ks} mutant allele harbours a 10 bp frameshift insertion at amino acid 80, encoding 15 out-of-frame amino acids until termination at 95 amino acids in length (Fig. 1A,B). In all three instances, the mutated forms of Nppa and Nppb lack the C-terminal region of the protein, which contains the mature peptides produced following processing (Fig. 1B) (Bloch et al., 1985). Given that targeting the propeptide region of Nppa has previously been shown to result in undetectable amounts of Nppa protein (John et al., 1995), we surmise that the *nppa*^{uq19ks}, *nppb*^{uq20ks} and *nppb*^{uq21ks} alleles are functional nulls.

The incross of *nppa*$^{+/uq19ks}$ and *nppb*$^{+/uq21ks}$ single carriers generated embryos that, at the developmental stages analysed [48, 72 and 96 h post fertilisation (hpf)], appeared wild type, thus in line with the absence of phenotype in *Nppa*$^{-/-}$ and *Nppb*$^{-/-}$ mouse embryos as well as zebrafish single morphants (Becker et al., 2014; John et al., 1995; Tamura et al., 2000). In contrast, double homozygous *nppa*$^{uq19ks/uq19ks}$/*nppb*$^{uq20ks/uq20ks}$ embryos displayed pericardial oedema starting at 48 hpf (Fig. 1D-H). The penetrance of the phenotype was incomplete and the expressivity variable. Approximately 20% of double mutants presented a wild-type phenotype and, in the remaining 80% of the genotypically mutant embryos, pericardial oedema was accompanied by additional cardiac abnormalities, such as looping defects or blood regurgitation at the inflow tract, or both (Fig. 1H; Movie 1). One day later, the penetrance increased (Fig. 1H). These data confirm that Nppa and Nppb do indeed function redundantly and play a role during vertebrate cardiac development.

To establish whether compensation at the level of gene expression exists between *nppa* and *nppb*, we performed *in situ* hybridisation expression analysis on both single and double mutant embryos (Fig. 1C, Fig. S1). The intensity of both *nppa* or *nppb* staining was unaltered at all stages and genotypes analysed, with the exception of *nppb* (Fig. 1C and Fig. S1). To quantify the expression of *nppa* and *nppb* levels in order to address the issue of compensation, we performed Q-PCR analysis on single *nppa* and *nppb* mutant embryos compared with wild-type sibling controls. No significant difference was observed for any groups tested (Fig. S1). This

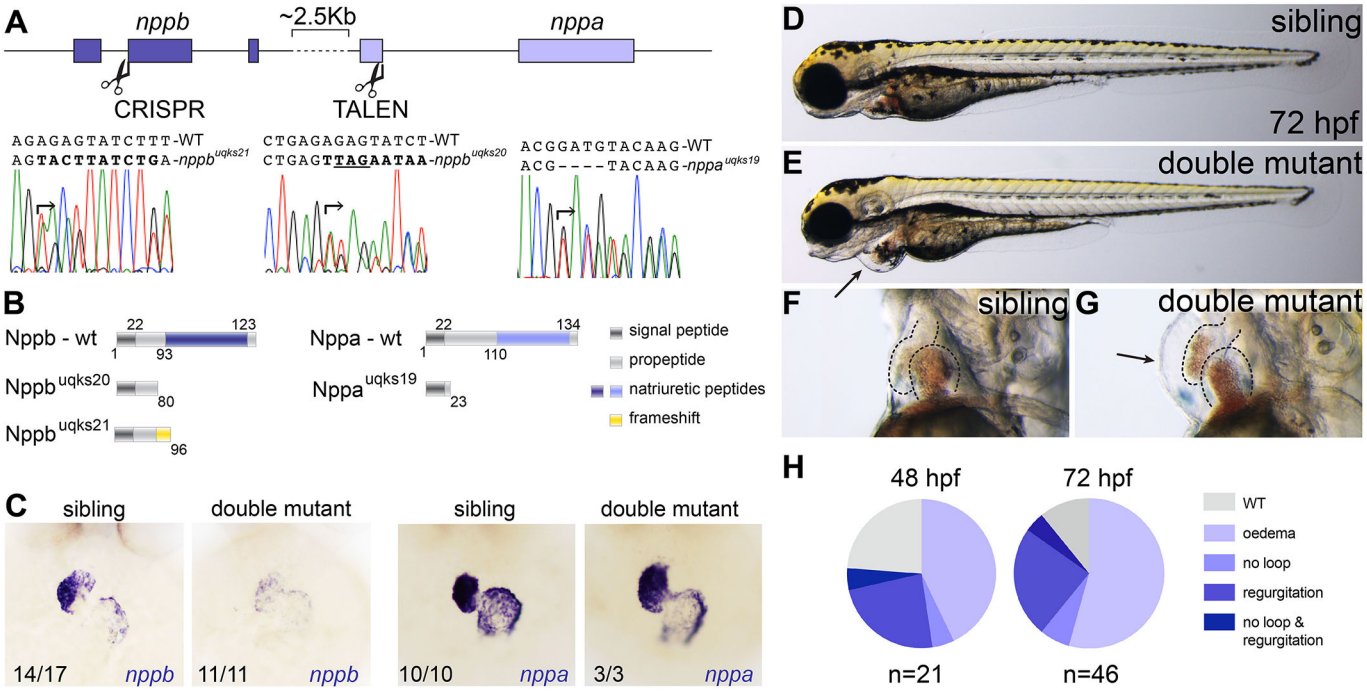

Fig. 1. Nppa and Nppb play redundant roles during early cardiac development. (A) Schematic of the zebrafish *nppb* and *nppa* gene cluster (on chromosome 8) and respective *nppb* CRISPR/Cas9 (base pair 239) and *nppa* TALEN cleavage sites (base pair 54). Sanger sequencing show three alleles of *nppa* and *nppb* genes identified following genome editing (*nppa*^{uq19ks}, *nppb*^{uq20ks} and *nppb*^{uq21ks}). (B) Schematics of Nppa and Nppb wild-type and mutant proteins. Numbers indicate predicted amino acid positions. (C) *In situ* hybridisation for *nppa* and *nppb* on sibling and double mutant embryos at 48 hpf demonstrate overtly wild-type morphology of double mutant hearts. *nppa* gene expression is unaltered in double mutants, whereas *nppb* appears decreased in double mutants. (D-G) Lateral bright-field images of representative 72 h post-fertilisation (hpf) sibling and double mutant embryos. Black arrow indicates the pericardial oedema observed in double mutants. (H) Pie charts illustrate the penetrance and expressivity of the phenotype at 48 hpf and 72 hpf.

Development (2018) 145, dev160739. doi:10.1242/dev.160739

demonstrates that there is no compensation occurring for these genes and is consistent with reports that *nppa* and *nppb* are co-regulated (Becker et al., 2012; Sergeeva et al., 2016, 2014).

Cardiomyocyte number and size, and cardiac output are all unchanged in double mutants

Previous studies inhibiting *nppa* and *nppb* expression via double morpholino knockdown have described increased cardiomyocyte numbers in double morphant embryos (Becker et al., 2014). To examine whether we observe a difference in cardiomyocyte number in double mutant versus sibling embryos, we crossed double heterozygous carriers onto the *Tg(myl7:dsRed-nls)* background (labelling cardiomyocyte nuclei) and quantified cell number from confocal *z*-stack images. In contrast to double morpholino-treated embryos, we observed no significant difference in cardiomyocyte number in double mutant embryos compared with siblings (Fig. 2A,A′).

Natriuretic peptides are well known for counteracting cardiac hypertrophy (Lerman et al., 1993; Vanderheyden et al., 2004) and, conversely, mice null for *Nppa* or the receptor shared by Nppa and Nppb, *Npr1*, display cardiac enlargement and augmented cardiomyocyte diameter (Ellmers et al., 2007; Holtwick et al., 2003; John et al., 1995). Quantifying cardiomyocyte size in double mutant hearts compared with siblings demonstrated no difference between double mutants and siblings (Fig. 2B,B′). Although this result is in contrast with that observed in $Nppa^{-/-}$ and $Npr1^{-/-}$ mice, these previous studies examine effects after months of *Nppa* deficiency (Ellmers et al., 2007; John et al., 1995). It is perhaps this chronic loss of Nppa signalling that accounts for the discrepancy between our work and previous reports.

Next, to investigate heart function of double mutants, high-speed imaging of siblings and double mutants was performed. By observing movies of siblings versus double mutant hearts, blood flow appeared slower when examining the inflow tract of beating hearts, which would account for the pericardial oedema observed in double mutant embryos (Movie 1). However, quantitative measurements of stroke volume and ejection fraction showed no significant difference between sibling and mutant embryos (Fig. S2). These measurements rely on comparable morphology between different groups being measured. Considering the distention of the hearts observed from pericardial oedema, this is likely to have impaired measurements and may account for the lack of functional difference detected between siblings and mutants.

AVC markers are expanded and the cardiac jelly appears thicker in double mutant embryos

Given the repressive role *Tbx2* plays on *Nppa* expression (Christoffels et al., 2004; Habets et al., 2002), we sought to investigate whether a reciprocal repressive function for Nppa on AVC-restricted gene expression takes place. To examine this, we performed *in situ* hybridisation analysis for a range of AVC markers in sibling and double mutant embryos. Interestingly, expression of all markers tested, namely *bmp4*, *tbx2b*, *has2* and *versican*, was expanded in double mutant embryos at 72 hpf (Fig. 2C,D). To investigate whether this resulted in a concomitant increase in the number of cells transitioning to endocardial cushion (EC) identity, immunostaining for Alcama on the *Tg(fli1a:nEGFP)*^{y7} transgenic line was performed and EC cell number quantified. Surprisingly, no significant difference was observed in the number of EC cells between sibling and double mutant embryos (Fig. S3). Instead, the expansion of AVC marker gene expression appears to affect thickening of the jelly between the layers of the cardiac wall. When high-speed movies from Fig. S2 and Movie 1 were examined closely, an increased endocardial-to-myocardial thickness was consistently observed in double mutant embryos. To quantify this,

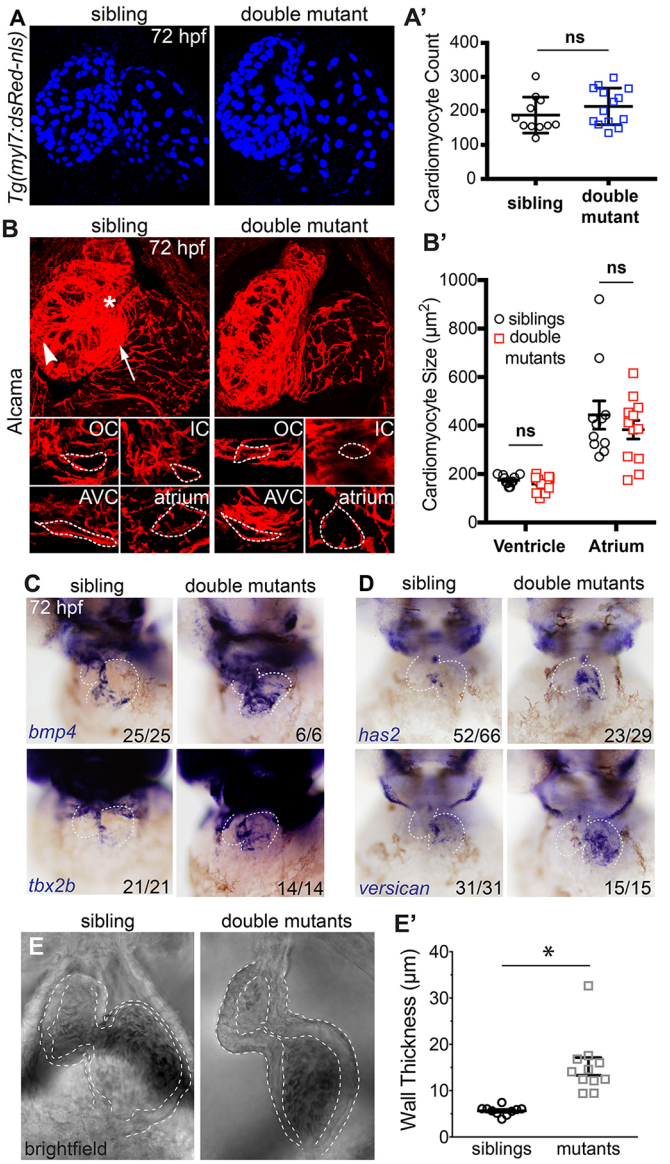

Fig. 2. AVC markers are expanded in double mutant embryos and cardiac jelly is thicker. (A) Confocal *z*-stacks of *Tg(myl7:dsRed-nls)* embryos (labelling cardiomyocyte nuclei) show no difference in cell number between sibling and double mutant embryos. (A′) Graphical representation of cell number (n=11 siblings; n=14 mutants). (B) Confocal images of representative sibling and double mutant embryos immunostained for Alcama to visualise cell shape. IC, inner curvature (white asterisk); OC, outer curvature (white arrowhead); AVC, atrioventricular canal (white arrow). Individual cardiomyocytes are outlined with broken lines. (B′) Graph showing average cardiomyocyte size of ventricle and atrium in siblings and double mutants (n=11 siblings; n=12 mutants). (C) *In situ* hybridisation analysis of AVC markers *bmp4*, *tbx2b*, *has2* and *versican* are expanded into the atrial chamber of double mutants compared with siblings. (E) Bright-field still images from high-speed movies of hearts at atrial diastole show thickened space (outlined) between the myocardial outer surface and the lumen surface of the heart, indicating thicker cardiac jelly in double mutants. (E′) Quantification of cardiac jelly thickness showing a significant increase in double mutant embryos compared with wild-type siblings when measuring the outer atrial myocardial wall and the inner luminal lining (n=10 siblings; n=11 mutants). ns, not significant; *P<0.05, as determined by *t*-test. Data are mean±s.d.

Development (2018) 145, dev160739. doi:10.1242/dev.160739

the area from the outer surface of the atrial myocardium to the luminal surface of the heart was measured and a significant difference was observed between sibling and double mutant embryos (Fig. 2E,E′).

ssNcan-GFP is a biosensor for the cardiac jelly

We recently reported a genetically encoded biosensor to detect HA in the developing embryo (De Angelis et al., 2017), using a similar approach used in cultured cells (Zhang et al., 2004). This biosensor uses the HA-binding domain of the protein, Neurocan, fused to EGFP with a synthetic secretion sequence to export it extracellularly and localise it to HA. Given that HA is a major component of the cardiac jelly, we applied this tool to examine double mutant embryos. Although transient mRNA injection could be used for analysing early stages of zebrafish development, we found poor reproducibility by 48 hpf in the cardiac jelly. We therefore generated a stable transgenic line, *Tg(ubi:ssNcan-EGFP)*^{uq25bh}, using the *ubiquitin* (*ubi*) promoter and observed robust and reproducible localisation of EGFP in the cardiac jelly (Fig. 3 and Movie 2). To validate that ssNcan-EGPF was indeed indicative of HA localisation and not simply an accumulation of secreted protein, we generated a ubiquitously expressing secreted GFP transgenic line [*Tg(ubi:ssEGFP)*^{uq7ks}] and found that, not only did it have different GFP localisation from *Tg(ubi:ssNcan-EGFP)*, but almost no GFP was detected in the cardiac jelly (Fig. 3 and Movie 2), substantiating the use of the *Tg(ubi:ssNcan-EGFP)* line as a biosensor for HA and the cardiac jelly.

The cardiac jelly is increased in *nppa*/*nppb* double mutant hearts

To measure the cardiac jelly phenotype observed in Fig. 2E, we crossed double *nppa/nppb* carriers onto the *Tg(ubi:ssNcan-EGFP)* background and took confocal *z*-stacks of the hearts of anaesthetised live zebrafish. An obvious expansion of the fluorescent area was observed in double mutant embryos. Quantification showed a significant increase in ssNcan-EGFP area in the atrium but not ventricle of double mutants compared with siblings (Fig. 4A,B). Interestingly, this correlated with the region of AVC marker gene expansion: into the atrium but not the ventricle. Of note, this included the ECM-synthetic genes *has2* and *vesican*. *In vivo* and *in vitro* models have previously demonstrated that Nppa and Nppb exert anti-fibrotic function by inhibiting TGF-β-mediated fibroblast transformation and the production of ECM proteins (Ellmers et al., 2007; Horio et al., 2003; Li et al., 2008; Tamura et al., 2000; Tsuruda et al., 2002; Wang et al., 2003). We show here, that Nppa and Nppa exert a similar effect on ECM production during cardiac development.

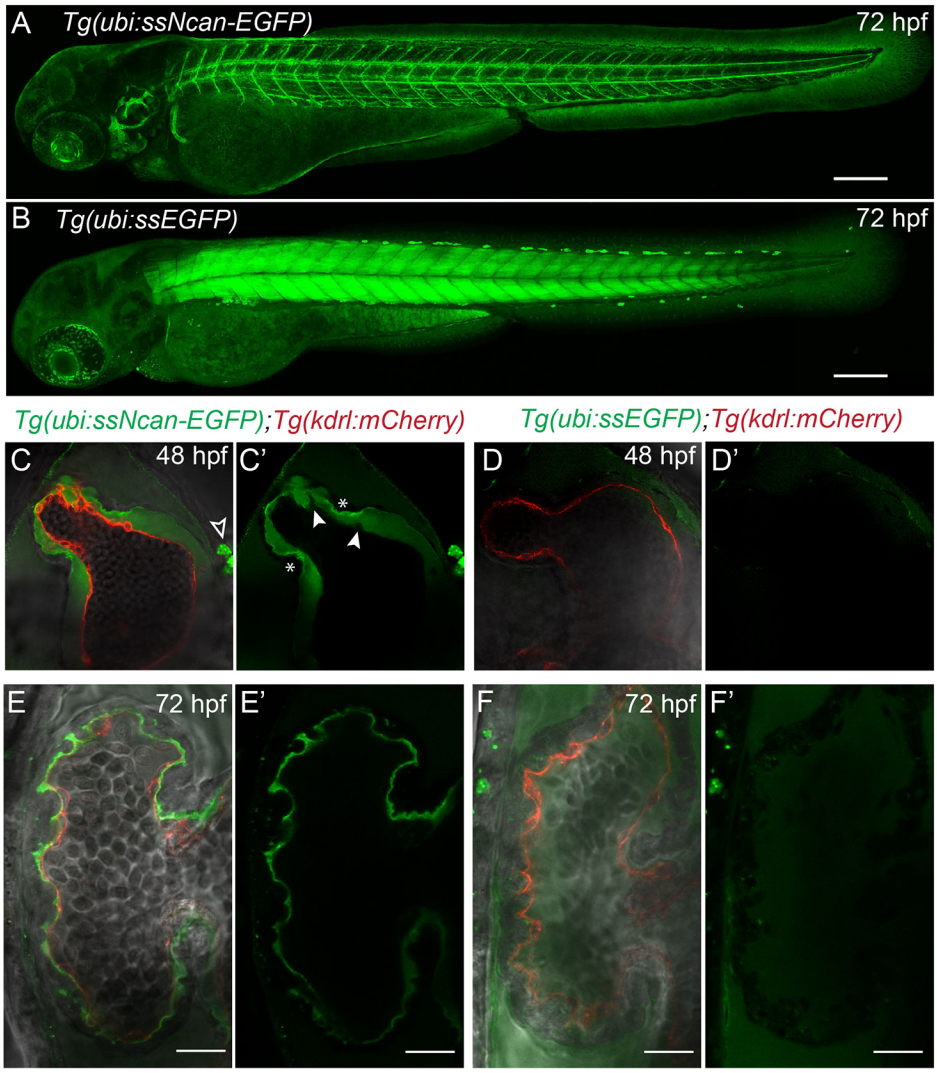

Fig. 3. A transgenic biosensor for the cardiac jelly. (A) Lateral view of the *Tg(ubi:ssNcan-EGFP)* line: a biosensor for hyaluronic acid – a major constituent of the cardiac jelly. The sensor expresses a secreted fusion protein of the HA-binding domain of Neurocan fused to GFP, driven by the *ubi* promoter. The biosensor localises to regions of HA, including the cardiac jelly, the otic vesicle and around the vasculature. (B) The *Tg(ubi:ssEGFP)* control was also generated and shows different EGFP localisation, predominantly to the skeletal muscle. Scale bars: 100 µm. (C,C′) Frontal view images of 48 hpf *Tg(ubi:ssNcan-EGFP)*/*Tg(kdrl:mCherry)* hearts anaesthetised and live imaged showing the cardiac jelly (green) and endocardial layer (red). ssNcan-EGFP localises to mucous cells (black arrowhead) and is concentrated at the AVC (asterisks). Regions devoid of ssNcan-EGFP in the cardiac jelly due to protruding endocardial cells can also be observed (white arrowheads). (D,D′) Live images of 48 hpf *Tg(ubi:ssEGFP)*/*Tg(kdrl:mCherry)* hearts showing near undetectable amounts of ssEGFP localisation (for full *z*-stacks of C,D, see Movie 2). (E,E′) Live images of 72 hpf *Tg(ubi:ssNcan-EGFP)*/*Tg(kdrl:mCherry)* ventricles showing condensed jelly and sites of trabeculae formation. (F,F′) Live images of 72 hpf *Tg(ubi:ssEGFP)*/*Tg(kdrl:mCherry)* hearts showing ssEGFP localisation in the pericardial space. Scale bar: 20 µm.

Development (2018) 145, dev160739. doi:10.1242/dev.160739

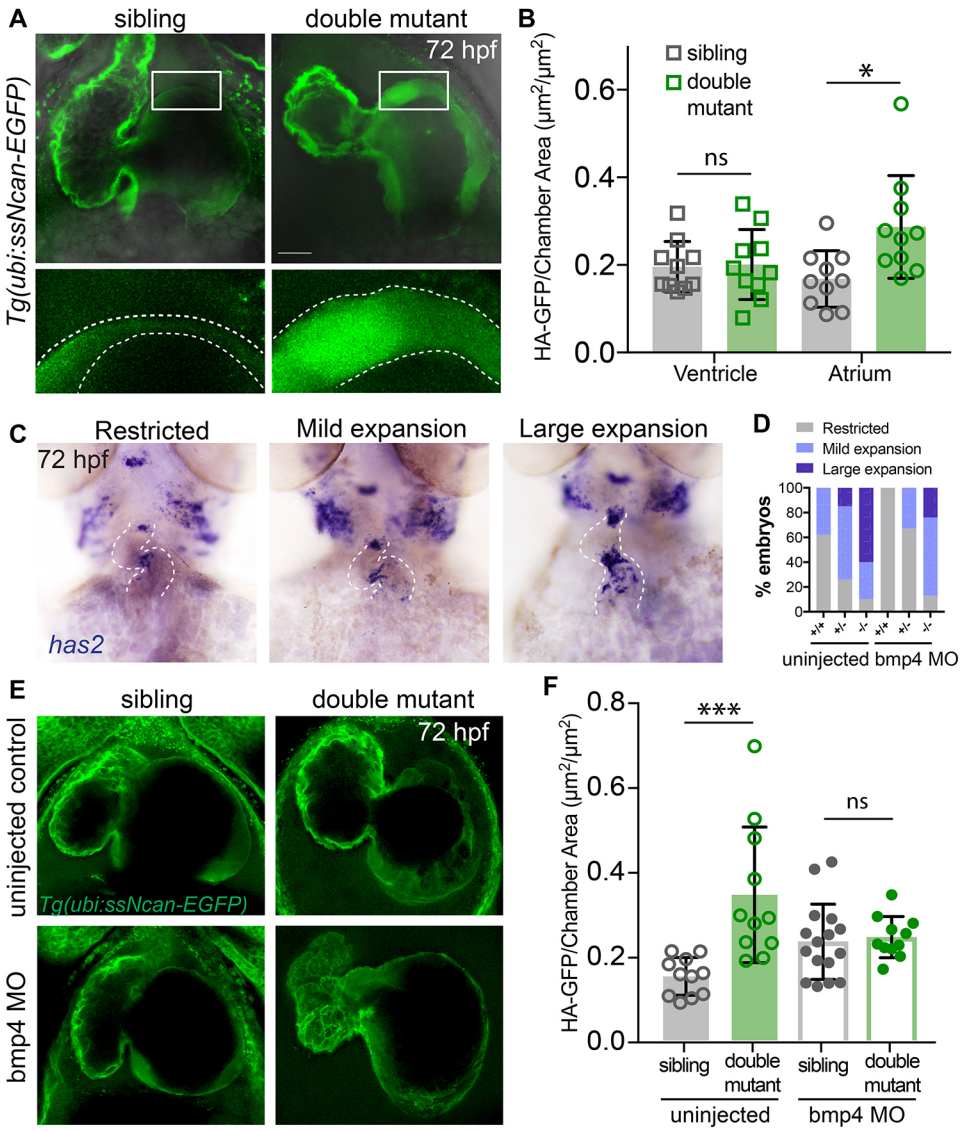

Fig. 4. The amount of cardiac jelly is increased in double mutant embryos and the AVC expansion is downstream of Bmp4 signalling. (A) Representative confocal stacks of the cardiac jelly in siblings versus double mutant embryos (ventral view, head towards the top), demonstrating thicker cardiac jelly (outlined) in double mutant embryos at 72 hpf. (B) Dot plot depicting the measurement of cardiac jelly area, showing no significant difference (ns) in jelly thickness of ventricles of siblings versus mutants, whereas significantly more jelly in the atrium of double mutants compared with siblings is observed (n=10; *P<0.05; two-tailed t-test). Data are mean±s.d. (C) Representative images of embryos following *in situ* hybridisation for *has2* expression in sibling and double mutant embryos. Images show categories of *has2* expression in embryos at 72 hpf. The heart is outlined. (D) The proportion of embryos with different categories of *has2* expression in wild-type (n=13), double heterozygotes (n=34) and double mutant (n=10) embryos in uninjected controls or in wild-type (n=5), double heterozygotes (n=9) and double mutant (n=8) embryos following *bmp4* knockdown. The proportion of phenotypes in double mutant embryos injected with *bmp4* morpholino most closely resembles uninjected double heterozygotes, demonstrating restoration of *has2* expression upon *bmp4* knockdown. (E) Representative confocal stacks of *Tg(ubi:ssNcan-EGFP)* to visualise the cardiac jelly in siblings versus double mutant embryos at 72 hpf, either uninjected or injected with *bmp4* morpholino. (F) Dot plots depicting the measurement of cardiac jelly area in atria of sibling versus double mutant embryos. A significant increase in the jelly area is observed between uninjected siblings and double mutants (n=11; ***P<0.01; two-way ANOVA for multiple comparisons with Tukey's *post hoc* correction). No significant difference (ns) is observed in the jelly area between siblings and double mutants following *bmp4* morpholino injection (n=16 siblings; n=11 double mutants), demonstrating that the increase in the cardiac jelly thickness is restored following *bmp4* morpholino injection. Two-tailed t-test; data are mean±s.d. Scale bar: 30 µm.

Existence of a regulatory loop between Nppa/Nppb, Bmp4 and Tbx2

Given the observed increase in *bmp4* expression in *nppa/nppb* double mutants and the knowledge that *has2* expression is downstream of Bmp signalling (Shirai et al., 2009), we investigated whether inhibition of Bmp signalling is sufficient to rescue the *has2* expansion in double mutants. We injected previously published *bmp4* morpholinos (Chocron et al., 2007) into a clutch of incrossed double heterozygous carriers, grew them until 72 hpf, performed *has2 in situ* hybridisation, imaged and categorised embryos then genotyped them. We observed a robust expansion of *has2* into the atrial chamber of double mutant embryos (as observed in Fig. 2). However, *bmp4* knockdown rescued the *has2* expression pattern to that of uninjected sibling controls (Fig. 4C,D).

To investigate whether the expanded cardiac jelly in double mutants was also downstream of Bmp signalling, we injected *bmp4* morpholinos into *nppa/nppb* double mutants on the *Tg(ubi:ssNcan-EGFP)* background and measured cardiac jelly area. As observed

Development (2018) 145, dev160739. doi:10.1242/dev.160739

for *has2* gene expression, the increased area of cardiac jelly in the atrium was restored to that of siblings following *bmp4* knockdown. We repeated this analysis using DMH1, a chemical inhibitor of Bmp signalling and, again, observed the cardiac jelly area restored to that of siblings (Fig. S4). Together, these data suggest that *nppa/nppb* disruption results in ectopic *bmp4* transcription into the atrial chamber, and in a resultant increase in HA synthesis and production of cardiac jelly.

These data demonstrate that Nppa and Nppb are required to repress the AVC genetic program within the atrial chamber, providing complementarity to the activity of Tbx2b in the AVC, which represses the chamber genetic program, including *nppa* and *nppb*. This mutually exclusive repressive activity must assist in establishing a sharp boundary between these two tissue compartments. Presumably, these ligands perform this function via receptor-mediated signalling, although this remains to be tested. What is still unknown is how receptor-mediated signalling acts to repress *bmp4*. We show that Nppa/Nppb signalling functions to inhibit *bmp4* transcription in the chambers, repressing the Bmp>Tbx2>Has2 cascade. The most noteworthy outcome of *nppa/nppb* deficiency is increased transcription of the extracellular matrix components *versican* and overproduction of HA.

In summary, these data reveal a previously unappreciated role for Nppa and Nppb in cardiac development. Zebrafish *nppa/nppb* double mutants develop pericardial oedema as early as 48 hpf. The functional consequence of losing Nppa/Nppb is unrestricted AVC boundary establishment, resulting in ectopic production of cardiac jelly in the atrial chamber. This role for Nppa/Nppb in restricting the Bmp-Tbx2-Has2 pathway from the chamber to the AVC, places Nppa/Nppb in a regulatory loop with Tbx2, upstream of Bmp.

MATERIALS AND METHODS

Zebrafish lines and transgenesis

All zebrafish strains were maintained and animal work performed in accordance with the guidelines of the animal ethics committee at The University of Queensland, Australia. The previously published transgenic lines used are *Tg(myl7:dsRed-nls)* (Mably et al., 2003); *Tg(kdrl:mCherry)* (Hogan et al., 2009) and *Tg(fli1a:nEGFP)*^{y7} (Lawson and Weinstein, 2002). Generation of the *Tg(ubi:ssEGFP)* and *Tg(ubi:ssNcan-EGFP)* lines was performed by injecting 1 nl of 25 ng/µl purified plasmid DNA (constructs described by De Angelis et al., 2017) into single-cell stage embryos together with *tol2* transposase mRNA (25 ng/µl). Embryos expressing EGFP mosaically were selected and raised to adulthood, and screened for germline transmission to generate stable transgenic lines.

Genome editing

TALEN monomers (Table S2) for *nppa* were generated using the golden gate kit (Cermak et al., 2011), cloned into the pCS2TAL3RR and pCS2TAL3DD backbones, and transcribed as previously described (Dahlem et al., 2012). CRISPR gDNA (Table S2) and co-injection with *cas9* mRNA for targeting *nppb* was performed as described (Capon et al., 2017). Fish were screened by high-resolution melt analysis (HRMA) using a Viia7 Real-Time PCR System (Applied Biosystems) and F1 embryos carrying a 4 bp deletion and 10 bp insertion for *nppa* and *nppb*, respectively, were outcrossed to the wild-type strain to generate an F2 population. To generate double mutants, *nppa* homozygous fish were incrossed and *nppb* CRISPR/Cas9 RNA injected into embryos. F1 embryos identified with a 39 bp insertion for *nppb* were outcrossed to the wild-type strain to generate an F2 population. Primers for HRMA and sequencing of individual mutations are listed in Table S2.

In situ hybridisation and antibody staining and MO injections

In situ hybridisation analysis was carried out as previously described (Smith et al., 2011). Immunohistochemistry was performed as previously described (Smith et al., 2008). Antibody details are provided in Table S2. The splice-targeting *bmp4* MO was used as previously described (Chocron et al., 2007). The standard *p53* control MO from Gene Tools was used.

Q-PCR analysis

DNA was extracted from the trunk of 48 hpf individual embryos as previously described (Dahlem et al., 2012) and genotyped by PCR using primer sequences depicted in Table S1. Following amplification, digestion with *Bsr*GI-HF which cuts the wild-type sequence, was performed and successful digest resolved by agarose gel electrophoresis. *nppb* embryos were genotyped by PCR using primer sequences from Table S1, which amplify wild-type and mutant amplicons (10 bp or 39 bp insertion) resolved by electrophoresis on a 2.5% sodium boric acid gel (Brody and Kern, 2004) at 200 V.

RNA was subsequently extracted from the remaining head/heart from a pool of four mutants or wild-type siblings in triplicate using a Direct-zol kit (Zymol Research) as per the manufacturer's guidelines. qPCR for *nppa* and *nppb* was performed on a Viia 7 system (Applied Biosystems). Efficiency corrected data was normalised to the geometric average of *ef1α* and *rpl13* using GeNorm (Vandesompele et al., 2002) as previously described (Coxam et al., 2014).

DMH1 inhibitor treatment

DMH1 was dissolved in DMSO. The DMSO control and DMH1 in DMSO were diluted with E3 medium to a concentration of 1 µM. Embryos were dechorionated and incubated in either DMSO or DMH1 solutions for 24 h (from 48-72 hpf), their hearts stopped with Tricaine and live imaging performed.

Live and fixed tissue imaging

Whole-mount *in situ* hybridisation embryos were imaged using an Olympus BX51 Upright Microscope Stand with Olympus DP70 CCD camera (10× dry objective). Confocal imaging was performed on a Zeiss Axiovert 200 Inverted Microscope Stand with LSM 710 Meta Confocal Scanner using 20× and 40× dry objectives (Zeiss Zen 2012 Black Software). High-speed movies (100 fps) were acquired using a Nikon Ti-E Inverted Stand with Hamamatsu Flash 4.0 sCMOS camera (20× dry objective - NIS Elements 4.3 Software). Fixed and live embryos for confocal imaging, as well as live embryos for movie acquisition, were mounted in low-melting point 1% agarose (Sigma-Aldrich).

Assessment of wall thickness and HA staining extent

Wall thickness was measured from movie acquisitions. Files were opened with the ImageJ 2.0.0 Software and individual frames analysed. The inner surface (IS) of the heart (as delimited by the endocardium) was subtracted from the myocardium-lined outer surface, in order to obtain the overall cardiac wall area. This value was normalised against the overall perimeter, calculated as the arithmetic mean of inner and outer perimeters. For each embryo, the corresponding wall thickness was obtained by averaging the measurements of three consecutive beating events. The extent of HA staining in the atrium was measured from confocal acquisitions of *Tg(ubi:ssNcan-EGFP)* embryos, calculating the ratio of EGFP-labelled area out of the total chamber area. For each embryo, the final value was the average of three measurements on subsequent optical sections, chosen to be at the level of the atrioventricular canal (AVC) and inflow tract. As for the quantification of HA in the ventricle (see Fig. 4A,B), relevant sections were selected to allow as clear a visualisation of the chamber inner and outer outlines as possible, preferably at the level of the AVC.

Image and statistical analyses

Image analysis and quantification was performed using Fiji (ImageJ 2.0.0 Software). Measurements of cell size were conducted as previously described (Auman et al., 2007). All cellular measurements were performed on three cells per condition from at least three different embryos. Movie analyses to determine 'stroke volume' and 'ejection fraction' were performed as described previously (Bagatto and Burggren, 2006). For statistical analysis, Gaussian distribution of the data and equal

Development (2018) 145, dev160739. doi:10.1242/dev.160739

variance among groups was assumed although not formally tested. The unpaired, two-tailed Student's *t*-test or two-way ANOVA followed by Tukey's *post hoc* test for multiple comparisons was employed (Prism 7.0a Software), as reported in figure legends.

Acknowledgements

The *bmp4* morpholino was a kind gift from Jeroen Bakkers. Confocal microscopy was performed at the Australian Cancer Research Foundation's Cancer Ultrastructure and Function Facility at The University of Queensland, Brisbane, Queensland 4072, Australia. The Alcama antibody (zn-8) was obtained from the Developmental Studies Hybridoma Bank, created by the NICHD of the NIH and maintained at The University of Iowa, Department of Biology, Iowa City, IA 52242, USA.

Competing interests

The authors declare no competing or financial interests.

Author contributions

Conceptualization: D.R.G., A.K.L., N.I.B., B.M.H., K.A.S.; Methodology: D.R.G., A.K.L., J.E.D.A., J.D.S., A.J., N.Z., N.I.B., K.A.S.; Validation: J.E.D.A., J.D.S., K.A.S.; Formal analysis: D.R.G., J.E.D.A., A.J., N.Z., K.A.S.; Investigation: D.R.G., J.D.S., A.J., N.Z., K.A.S.; Resources: D.R.G., A.K.L., J.E.D.A., N.I.B., B.M.H., K.A.S.; Data curation: D.R.G., J.E.D.A., J.D.S., A.J., N.Z., K.A.S.; Writing - original draft: D.R.G., K.A.S.; Writing - review & editing: A.K.L., A.J., B.M.H.; Visualization: J.E.D.A., J.D.S., A.J.; Supervision: A.K.L., B.M.H., K.A.S.; Project administration: K.A.S.; Funding acquisition: B.M.H., K.A.S.

Funding

D.R.G. was supported by a University of Queensland International scholarship. A.K.L. was supported by a University of Queensland Postdoctoral Fellowship. B.M.H. was supported by a National Heart Foundation of Australia/National Health and Medical Research Council Career Development Fellowship (1083811). K.A.S. was part funded by an Australian Research Council Future Fellowship (FT110100496). The research was part funded by a National Health and Medical Research Council project grant (GNT1123456).

Supplementary information

Supplementary information available online at
http://dev.biologists.org/lookup/doi/10.1242/dev.160739.supplemental

References

Auman, H. J., Coleman, H., Riley, H. E., Olale, F., Tsai, H.-J. and Yelon, D. (2007). Functional modulation of cardiac form through regionally confined cell shape changes. *PLoS Biol.* **5**, e53.

Bagatto, B. and Burggren, W. (2006). A three-dimensional functional assessment of heart and vessel development in the larva of the zebrafish (Danio rerio). *Physiol. Biochem. Zool.* **79**, 194-201.

Becker, J. R., Robinson, T. Y., Sachidanandan, C., Kelly, A. E., Coy, S., Peterson, R. T. and MacRae, C. A. (2012). In vivo natriuretic peptide reporter assay identifies chemical modifiers of hypertrophic cardiomyopathy signalling. *Cardiovasc. Res.* **93**, 463-470.

Becker, J. R., Chatterjee, S., Robinson, T. Y., Bennett, J. S., Panakova, D., Galindo, C. L., Zhong, L., Shin, J. T., Coy, S. M., Kelly, A. E. et al. (2014). Differential activation of natriuretic peptide receptors modulates cardiomyocyte proliferation during development. *Development* **141**, 335-345.

Bloch, K. D., Scott, J. A., Zisfein, J. B., Fallon, J. T., Margolies, M. N., Seidman, C. E., Matsueda, G. R., Homcy, C. J., Graham, R. M. and Seidman, J. G. (1985). Biosynthesis and secretion of proatrial natriuretic factor by cultured rat cardiocytes. *Science* **230**, 1168-1171.

Brody, J. R. and Kern, S. E. (2004). Sodium boric acid: a Tris-free, cooler conductive medium for DNA electrophoresis. *BioTechniques* **36**, 214-216.

Camenisch, T. D., Spicer, A. P., Brehm-Gibson, T., Biesterfeldt, J., Augustine, M. L., Calabro, A., Jr, Kubalak, S., Klewer, S. E. and McDonald, J. A. (2000). Disruption of hyaluronan synthase-2 abrogates normal cardiac morphogenesis and hyaluronan-mediated transformation of epithelium to mesenchyme. *J. Clin. Invest.* **106**, 349-360.

Capon, S. J., Baillie, G. J., Bower, N. I., da Silva, J. A., Paterson, S., Hogan, B. M., Simons, C. and Smith, K. A. (2017). Utilising polymorphisms to achieve allele-specific genome editing in zebrafish. *Biol. Open* **6**, 125-131.

Cermak, T., Doyle, E. L., Christian, M., Wang, L., Zhang, Y., Schmidt, C., Baller, J. A., Somia, N. V., Bogdanove, A. J. and Voytas, D. F. (2011). Efficient design and assembly of custom TALEN and other TAL effector-based constructs for DNA targeting. *Nucleic Acids Res.* **39**, e82.

Chi, N. C., Shaw, R. M., De Val, S., Kang, G., Jan, L. Y., Black, B. L. and Stainier, D. Y. R. (2008). Foxn4 directly regulates tbx2b expression and atrioventricular canal formation. *Genes Dev.* **22**, 734-739.

Chocron, S., Verhoeven, M. C., Rentzsch, F., Hammerschmidt, M. and Bakkers, J. (2007). Zebrafish Bmp4 regulates left-right asymmetry at two distinct developmental time points. *Dev. Biol.* **305**, 577-588.

Christoffels, V. M., Hoogaars, W. M. H., Tessari, A., Clout, D. E. W., Moorman, A. F. M. and Campione, M. (2004). T-box transcription factor Tbx2 represses differentiation and formation of the cardiac chambers. *Dev. Dyn.* **229**, 763-770.

Coxam, B., Sabine, A., Bower, N. I., Smith, K. A., Pichol-Thievend, C., Skoczylas, R., Astin, J. W., Frampton, E., Jaquet, M., Crosier, P. S. et al. (2014). Pkd1 regulates lymphatic vascular morphogenesis during development. *Cell Rep.* **7**, 623-633.

Dahlem, T. J., Hoshijima, K., Jurynec, M. J., Gunther, D., Starker, C. G., Locke, A. S., Weis, A. M., Voytas, D. F. and Grunwald, D. J. (2012). Simple methods for generating and detecting locus-specific mutations induced with TALENs in the zebrafish genome. *PLoS Genet.* **8**, e1002861.

De Angelis, J. E., Lagendijk, A. K., Chen, H., Tromp, A., Bower, N. I., Tunny, K. A., Brooks, A. J., Bakkers, J., Francois, M., Yap, A. S. et al. (2017). Tmem2 regulates embryonic Vegf signaling by controlling hyaluronic acid turnover. *Dev. Cell* **40**, 123-136.

Ellmers, L. J., Scott, N. J. A., Piuhola, J., Maeda, N., Smithies, O., Frampton, C. M., Richards, A. M. and Cameron, V. A. (2007). Npr1-regulated gene pathways contributing to cardiac hypertrophy and fibrosis. *J. Mol. Endocrinol.* **38**, 245-257.

Habets, P. E. M. H., Moorman, A. F. M., Clout, D. E. W., van Roon, M. A., Lingbeek, M., van Lohuizen, M., Campione, M. and Christoffels, V. M. (2002). Cooperative action of Tbx2 and Nkx2.5 inhibits ANF expression in the atrioventricular canal: implications for cardiac chamber formation. *Genes Dev.* **16**, 1234-1246.

Harrelson, Z., Kelly, R. G., Goldin, S. N., Gibson-Brown, J. J., Bollag, R. J., Silver, L. M. and Papaioannou, V. E. (2004). Tbx2 is essential for patterning the atrioventricular canal and for morphogenesis of the outflow tract during heart development. *Development* **131**, 5041-5052.

Hogan, B. M., Bos, F. L., Bussmann, J., Witte, M., Chi, N. C., Duckers, H. J. and Schulte-Merker, S. (2009). Ccbe1 is required for embryonic lymphangiogenesis and venous sprouting. *Nat. Genet.* **41**, 396-398.

Holtwick, R., van Eickels, M., Skryabin, B. V., Baba, H. A., Bubikat, A., Begrow, F., Schneider, M. D., Garbers, D. L. and Kuhn, M. (2003). Pressure-independent cardiac hypertrophy in mice with cardiomyocyte-restricted inactivation of the atrial natriuretic peptide receptor guanylyl cyclase-A. *J. Clin. Invest.* **111**, 1399-1407.

Horio, T., Tokudome, T., Maki, T., Yoshihara, F., Suga, S.-I., Nishikimi, T., Kojima, M., Kawano, Y. and Kangawa, K. (2003). Gene expression, secretion, and autocrine action of C-type natriuretic peptide in cultured adult rat cardiac fibroblasts. *Endocrinology* **144**, 2279-2284.

Inoue, K., Naruse, K., Yamagami, S., Mitani, H., Suzuki, N. and Takei, Y. (2003). Four functionally distinct C-type natriuretic peptides found in fish reveal evolutionary history of the natriuretic peptide system. *Proc. Natl. Acad. Sci. USA* **100**, 10079-10084.

John, S. W., Krege, J. H., Oliver, P. M., Hagaman, J. R., Hodgin, J. B., Pang, S. C., Flynn, T. G. and Smithies, O. (1995). Genetic decreases in atrial natriuretic peptide and salt-sensitive hypertension. *Science* **267**, 679-681.

Keyes, W. M., Logan, C., Parker, E. and Sanders, E. J. (2003). Expression and function of bone morphogenetic proteins in the development of the embryonic endocardial cushions. *Anat. Embryol. (Berl)* **207**, 135-147.

Lawson, N. D. and Weinstein, B. M. (2002). In vivo imaging of embryonic vascular development using transgenic zebrafish. *Dev. Biol.* **248**, 307-318.

Lerman, A., Gibbons, R. J., Rodeheffer, R. J., Bailey, K. R., McKinley, L. J., Heublein, D. M. and Burnett, J. C. Jr. (1993). Circulating N-terminal atrial natriuretic peptide as a marker for symptomless left-ventricular dysfunction. *Lancet* **341**, 1105-1109.

Li, P., Wang, D., Lucas, J., Oparil, S., Xing, D., Cao, X., Novak, L., Renfrow, M. B. and Chen, Y.-F. (2008). Atrial natriuretic peptide inhibits transforming growth factor beta-induced Smad signaling and myofibroblast transformation in mouse cardiac fibroblasts. *Circ. Res.* **102**, 185-192.

Ma, L., Lu, M. F., Schwartz, R. J. and Martin, J. F. (2005). Bmp2 is essential for cardiac cushion epithelial-mesenchymal transition and myocardial patterning. *Development* **132**, 5601-5611.

Mably, J. D., Mohideen, M. A., Burns, C. G., Chen, J.-N. and Fishman, M. C. (2003). heart of glass regulates the concentric growth of the heart in zebrafish. *Curr. Biol.* **13**, 2138-2147.

Sergeeva, I. A., Hooijkaas, I. B., Van Der Made, I., Jong, W. M. C., Creemers, E. E. and Christoffels, V. M. (2014). A transgenic mouse model for the simultaneous monitoring of ANF and BNP gene activity during heart development and disease. *Cardiovasc. Res.* **101**, 78-86.

Sergeeva, I. A., Hooijkaas, I. B., Ruijter, J. M., van der Made, I., de Groot, N. E., van de Werken, H. J. G., Creemers, E. E. and Christoffels, V. M. (2016).

Identification of a regulatory domain controlling the Nppa-Nppb gene cluster during heart development and stress. *Development* **143**, 2135-2146.

Shirai, M., Imanaka-Yoshida, K., Schneider, M. D., Schwartz, R. J. and Morisaki, T. (2009). T-box 2, a mediator of Bmp-Smad signaling, induced hyaluronan synthase 2 and Tgfbeta2 expression and endocardial cushion formation. *Proc. Natl. Acad. Sci. USA* **106**, 18604-18609.

Smith, K. A., Chocron, S., von der Hardt, S., de Pater, E., Soufan, A., Bussmann, J., Schulte-Merker, S., Hammerschmidt, M. and Bakkers, J. (2008). Rotation and asymmetric development of the zebrafish heart requires directed migration of cardiac progenitor cells. *Dev. Cell* **14**, 287-297.

Smith, K. A., Lagendijk, A. K., Courtney, A. D., Chen, H., Paterson, S., Hogan, B. M., Wicking, C. and Bakkers, J. (2011). Transmembrane protein 2 (Tmem2) is required to regionally restrict atrioventricular canal boundary and endocardial cushion development. *Development* **138**, 4193-4198.

Tamura, N., Ogawa, Y., Yasoda, A., Itoh, H., Saito, Y. and Nakao, K. (1996). Two cardiac natriuretic peptide genes (atrial natriuretic peptide and brain natriuretic peptide) are organized in tandem in the mouse and human genomes. *J. Mol. Cell. Cardiol.* **28**, 1811-1815.

Tamura, N., Ogawa, Y., Chusho, H., Nakamura, K., Nakao, K., Suda, M., Kasahara, M., Hashimoto, R., Katsuura, G., Mukoyama, M. et al. (2000). Cardiac fibrosis in mice lacking brain natriuretic peptide. *Proc. Natl. Acad. Sci. USA* **97**, 4239-4244.

Tien, J. Y. L. and Spicer, A. P. (2005). Three vertebrate hyaluronan synthases are expressed during mouse development in distinct spatial and temporal patterns. *Dev. Dyn.* **233**, 130-141.

Tsuruda, T., Boerrigter, G., Huntley, B. K., Noser, J. A., Cataliotti, A., Costello-Boerrigter, L. C., Chen, H. H. and Burnett, J. C. Jr. (2002). Brain natriuretic Peptide is produced in cardiac fibroblasts and induces matrix metalloproteinases. *Circ. Res.* **91**, 1127-1134.

Vanderheyden, M., Goethals, M., Verstreken, S., De Bruyne, B., Muller, K., Van Schuerbeeck, E. and Bartunek, J. (2004). Wall stress modulates brain natriuretic peptide production in pressure overload cardiomyopathy. *J. Am. Coll. Cardiol.* **44**, 2349-2354.

Vandesompele, J., De Preter, K., Pattyn, F., Poppe, B., Van Roy, N., De Paepe, A. and Speleman, F. (2002). Accurate normalization of real-time quantitative RT-PCR data by geometric averaging of multiple internal control genes. *Genome Biol.* **3**, RESEARCH0034.

Verhoeven, M. C., Haase, C., Christoffels, V. M., Weidinger, G. and Bakkers, J. (2011). Wnt signaling regulates atrioventricular canal formation upstream of BMP and Tbx2. *Birth Defects Res. A Clin. Mol. Teratol* **91**, 435-440.

Walsh, E. C. and Stainier, D. Y. (2001). UDP-glucose dehydrogenase required for cardiac valve formation in zebrafish. *Science* **293**, 1670-1673.

Wang, D., Oparil, S., Feng, J. A., Li, P., Perry, G., Chen, L. B., Dai, M., John, S. W. M. and Chen, Y.-F. (2003). Effects of pressure overload on extracellular matrix expression in the heart of the atrial natriuretic peptide-null mouse. *Hypertension* **42**, 88-95.

Zhang, H., Baader, S. L., Sixt, M., Kappler, J. and Rauch, U. (2004). Neurocan-GFP fusion protein: a new approach to detect hyaluronan on tissue sections and living cells. *J. Histochem. Cytochem.* **52**, 915-922.